POLITECNICO DI TORINO
Repository ISTITUZIONALE

Experimental analysis and preliminary model of non-conventional lip seals

Original
Experimental analysis and preliminary model of non-conventional lip seals / Raparelli, Terenziano; Mazza, Luigi; Trivella, Andrea. - In: TRIBOLOGY INTERNATIONAL. - ISSN 0301-679X. - 181:108311(2023).

Availability:
This version is available at: 11583/2977412 since: 2023-03-29T11:27:17Z

Publisher:
Elsevier

Published
DOI:

Terms of use:
openAccess

This article is made available under terms and conditions as specified in the corresponding bibliographic description in the repository

Publisher copyright
Elsevier preprint/submitted version

(Article begins on next page)

12 June 2023

Experimental analysis and preliminary model of non-conventional lip seals

Terenziano Raparelli, Luigi Mazza, Andrea Trivella
Department of Mechanical and Aerospace Engineering
Politecnico di Torino, Torino, Italy

Abstract
The paper describes the tests carried out to determine the applicability of a simple means for reducing friction force in linear pneumatic actuators. The idea is based on the use of commercial lip seals mounted in the direction opposite to that used in conventional systems. Two different non-conventional installations were tested using commercial spring-energized seals consisting of two different materials: virgin PTFE and graphite-filled PTFE. Tests assessed the effect of bore manufacturing tolerances with nominal bore diameters of 50.0 mm and 50.2 mm. Performance was evaluated in terms of leakage flow rate and friction force, comparing the proposed installation with conventionally mounted seals. Moreover, friction coefficient and stiffness of the two seal materials were measured on a seal segment mounted on a pin-on-disk tribometer implemented with a special pin design; tests were carried out by loading the seal segment against a portion of the cylinder barrel in reciprocating motion. Stiffness and friction coefficient measurements served as the basis for developing a preliminary lumped parameter model of the lip seal which was used to analyze lip deflections, exchanged forces and leakage flow rate between seal and barrel.

Keywords: lip seals, pneumatics, tribometer, lumped parameters model, leakage

1 Introduction

Pneumatic cylinders are widely used in sliding applications. They normally feature lip seals installed in the piston to prevent air from passing between the two cylinder chambers, or on the rod to prevent leakage between the front chamber and the outside environment. Seal configuration and materials are such that chamber pressure ensures good contact with bore and rod surface. While this contact guarantees that a seal can be established, it also creates friction forces that lead to energy losses and wear that over time reduce sealing performance and thus make regular maintenance and replacement necessary. To overcome these shortcomings and minimize seal friction forces, the literature offers studies of optimized cross sections [1-4] and low-friction materials and coatings for rubber seals [5-8]. To operate correctly, conventional seals, i.e., those based on contact between seal and counterpart, must be grease lubricated [3-4]. However, such seals cannot be used in processes where the air in the working environment and the compressed air used in the cylinders must be absolutely free from contaminants. Processes of this kind are typical of the medical, pharmaceutical and food processing industries as well as the production and assembly of electronic components, and in many cases make use of cleanrooms. Consequently, pneumatic actuators have been under development in the last few years which operate without contact between piston and barrel, and thus permit small amounts of air leakage, on the principle of air-lubricated bearings. The absence or near absence of contact between parts in relative motion provides two major advantages, as greases and lubricants are not used and friction forces are reduced. In addition, the air gap in the sliding interface between the parts in relative motion acts as a lubricant.

One such design is analyzed in [9, 11], and features variable-profile pistons where the circumferential pressure distribution in the air gap between piston and barrel provides a self-centering action. A uniform-clearance pumping ring rod seal was investigated in [12], demonstrating the potential of the uniform-clearance design through a numerical example. Other designs employ piston rings with friction-reducing laser surface texturing [13, 14] which produces micro-dimples that act as bearings between the sliding surfaces. Using designs of this kind is not always economical, however, as they require precision fits and geometries. A non-conventional lip seal with pneumatic spring was designed and tested in [15]; results indicated that the seal performs well thanks to the self-tuning behavior of the internal pneumatic spring connected directly to supply pressure. Unfortunately, the design involves two seals integrated in a single assembly, and shapes and materials must be carefully selected.

A simpler and more economical alternative to these designs employs commercial lip seals installed on the piston in the direction opposite to that used in a conventional installation. In this way, the seals—and the lip in particular—are deflected by the chamber pressure, creating an air gap that provides a lubricating action and thus reduces the friction force. Though sealing between surfaces in relative motion is no longer total, as a slight amount of leakage is permitted, the leakage flow rate must be kept to acceptable levels. As described in [16], the feasibility of this approach has been tested using commercial and prototype seals with and without preload springs installed on a commercial cylinder. Performance in this

case was evaluated only in terms of leakage and friction, ignoring the effects of seat geometry changes and bore manufacturing tolerances, though they can have a significant impact. In addition to these factors, other design parameters that must be carefully chosen to ensure good sealing performance include seal installation preload, materials, and whether or not energizing springs are used. The effect of seal seat and bore manufacturing tolerances on leakage flow rate was investigated in [17] using the same commercial seal subjected to preliminary testing in [16]. In the non-conventional installation configuration, the tested seals showed a low leakage flow rate, but friction performance was not significantly better than that of conventionally installed seals because of the stiffness of the material and the energizing spring, and the effect of assembly tolerances.

This paper thus presents new non-conventionally mounted commercial seals which can ensure friction forces below those encountered with conventional installations. Tests were carried out on PTFE and graphite-filled PTFE lip seals for 50 mm bore cylinders. The seals were installed on the piston of a commercial actuator in order to measure friction forces and determine the effect of cylinder bore tolerances on leakage flow rate. In addition, friction coefficient and radial stiffness of the two seal lips were measured on a seal segment mounted on a pin-on-disk tribometer featuring a special pin design. Stiffness and friction coefficient measurements were used as the basis for developing a preliminary model of the seal lip. The following pages present the proposed installation on a commercial actuator, the tests carried out on the complete system and on the tribometer, and a comparison between the experimental results and those obtained with the model.

2 The non-conventional mounting system

A typical example of conventional lip seal installation on a double-acting pneumatic actuator is shown in Figure 1. Such seals have an excellent ability to achieve close contact with the barrel surfaces under the action of chamber pressure. This ensures excellent sealing, both across the chambers and with the atmosphere. Arrows A and B indicate chamber pressure acting on the sealing lip and barrel contact pressure respectively.

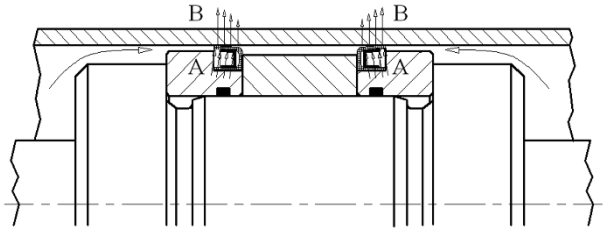

Figure 1: Conventional lip seal installation

The non-conventional installation is shown in Figure 2. Chamber pressure deflects the seal lips, allowing air to escape towards an exhaust hole in the piston which is large enough to ensure that pressure in the two cylinder chambers is completely decoupled. By deflecting, the seals reduce contact with the barrel, thus reducing the friction force. However, as the leakage flow rate must be kept to acceptable levels, the seals must be installed with an initial preload to prevent the cylinder pressure from opening the lips excessively.

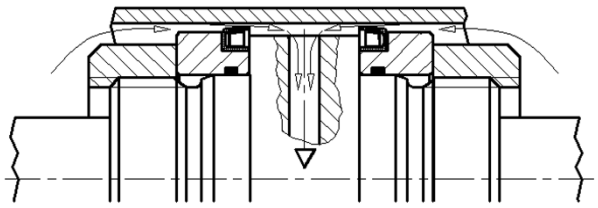

Figure 2: Non-conventional lip seal installation

Figure 3 shows the two types of commercial lip seal that were tested: Type A_1 (PTFE), and Type A_2 (graphite-filled PTFE. Both types have the same geometry and are energized by a metal cantilever spring.

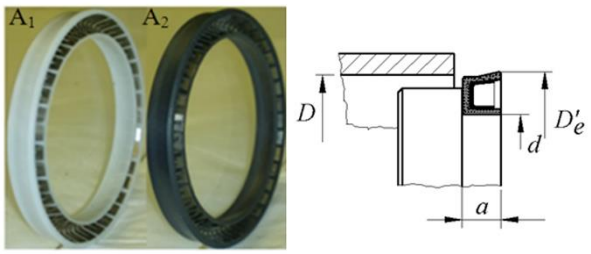

Figure 3: Commercial seals and main dimensions

Table 1: Seal and seat dimensions (mm)

	A_1	A_2
De'	51.24	51.32
d	40.56	
D	50.0 - 50.2	
a	6.71	
x_0	0.62 – 0.52	0.66 - 0.56

Table 1 shows axial width *a* and diameter *d* of the seal seat, outside diameter *De'* of the installed seal, bore diameters *D* and radial interference x_0. Barrels with different bore diameters were used to investigate the effects of assembly tolerance (+0.2 mm). Barrels are constructed of stainless steel, with a bore surface roughness of *Ra*=0.6 µm in all cases. These tolerance and roughness values are typical of 50 mm bore commercial pneumatic cylinders. Values shown for the seals are the averages of measurements taken on three specimens of the same type used for testing. Manufacturing tolerances are of major importance in radial lip seals as they are responsible for seal assembly interference, whose effects on the radial force at seal-counterpart interface cannot be neglected [18-20].

A cross-sectional view and a photograph of the piston under test are shown in Figure 4. Interchangeable rings (2) secured to piston (1) carry seats for lip seals (3). The piston-seal assembly is inserted in bore (4).
In a conventional installation, the seal lip faces pressure side p_1 so that pressure forces it into contact with bore (4), Here, by contrast, the assembly is "reversed", i.e., the lip faces in the direction opposite p_1. Seal deformability must provide a narrow gap between lip and bore, while the amount of leakage through the gap must be sufficiently small to reduce friction without excessive loss of air. A metal spring stiffens the seal. Air flow through the seal is exhausted through four radial holes (5) and axial port (6) machined in piston and rod.

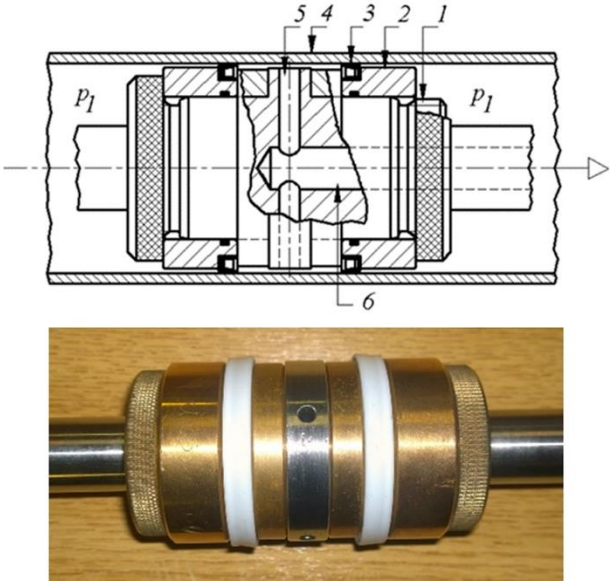

Figure 4: Cross section through piston and cylinder barrel and photograph of piston and seals

3 Testing

3.1 Leakage flow rate measurement

The test setup used to measure leakage flow rate discharged from pneumatic cylinder (1) is shown schematically in Figure 5 [21, 22]. Regulator (2) controls pressure p_1 in both chambers, which is measured by gauge (3). The piston with test seals is installed inside the cylinder barrel and secured axially by means of spacers placed in the barrel. Leakage across the test seal is exhausted via the axial port in the piston-rod assembly and measured by float-type flowmeter (4). Measurements were taken while varying supply pressure to the two cylinder chambers. Two readings were recorded for each installation position and then averaged.

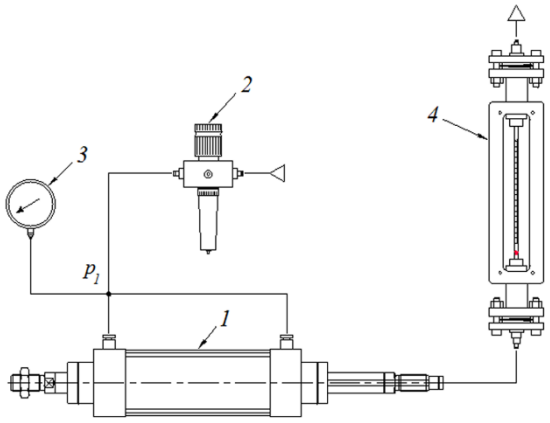

Figure 5: Leakage flow rate measurement setup

The first measurements indicated that for low radial interference values (see Table 1), the leakage flow rate reaches a peak and then drops, rather than increasing constantly along with supply pressure. This behavior was attributed to a combination of two effects of chamber pressure: the first is the desired effect whereby an air gap is created between lip and bore, while the second is due to axial seal movement in the seat which deflects the lip in the direction that narrows the gap. At supply pressures over 4 bar, the second effect predominates over the first, closing the gap sufficiently to reduce the leakage flow rate and thus increase friction force. This unwanted seal movement was prevented by securing the seal axially in the seat by means of a tapered ring as shown in Figure 6.

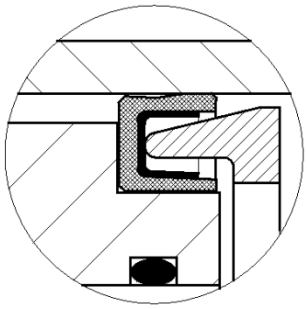
Figure 6: Tapered seal retaining ring

The tapered ring holds the seal sides firmly up against the seat shoulders, preventing uncontrolled movements while allowing the lip to deflect and open the air gap. In addition, firm contact with the seat prevents air from passing under the seal, i.e., along the seat shoulders, so that the entire air flow acts to open the gap between lip and barrel.
The graph in Figure 7a shows leakage flow rates at 6 bar supply pressure for seals A_1 and A_2, comparing the three seal installation configurations: conventional, non-conventional, and non-conventional with tapered ring.
As can be seen, for the non-conventional installation both with and without tapered ring, leakage flow rate is lower for graphite-filled PTFE seals A_2. This lower flow rate makes it more difficult for seal A_2 to deflect and open the air gap, and is due to the fact that seal A_2 is stiffer than virgin PTFE seal A_1. For the conventional installation, the greater stiffness of seal A_2 makes it harder for this seal to flex under the action of pressure against the barrel, i.e., in the direction which closes the air gap. This is confirmed by the higher leakage flow rate recorded for seal A_2 in the conventional installation (Figure 7a). The difference in stiffness is also apparent to the touch, as the lip will deflect under cantilever pressure. Figure 7b, on the other hand, shows the effect of bore manufacturing tolerances for seal A_1 in the non-conventional installation configuration. As can be seen, the seal is very sensitive to the increase in diameter, as the leakage flow rate is three times that measured with the nominal diameter at the same supply pressure.

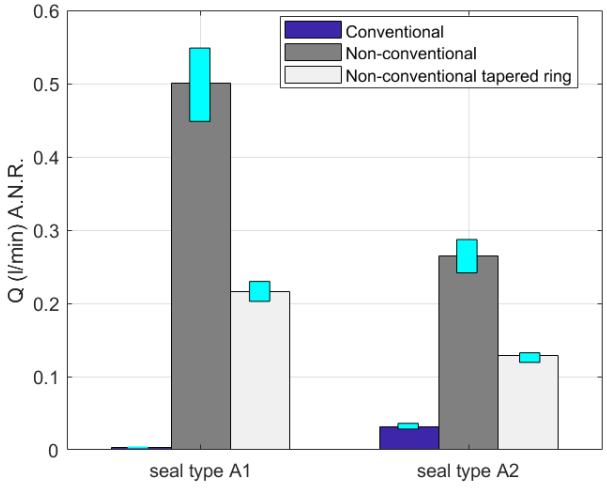

a)

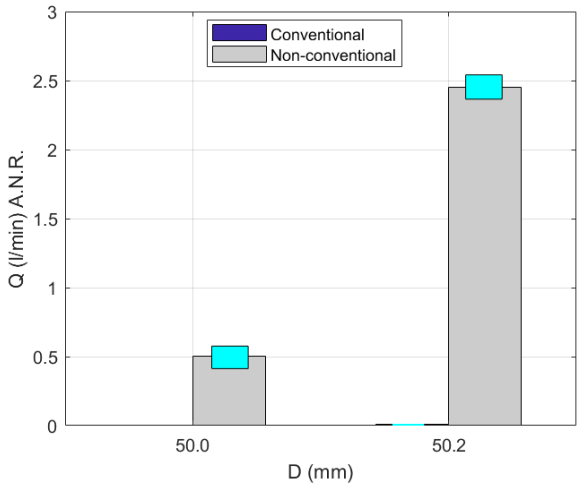

b)

Figure 7: Leakage flow rate with 6 bar supply pressure a) in different installation conditions; b) effect of bore manufacturing tolerances

Figure 8 shows flow rate measurements with seals A_1 and A_2 installed on both sides of the piston (double seal, non-conventional mounting with tapered ring) as supply pressure $p_1$rises. Correct system operation is demonstrated by the fact that flow rate increases along with supply pressure, with no sudden drops.

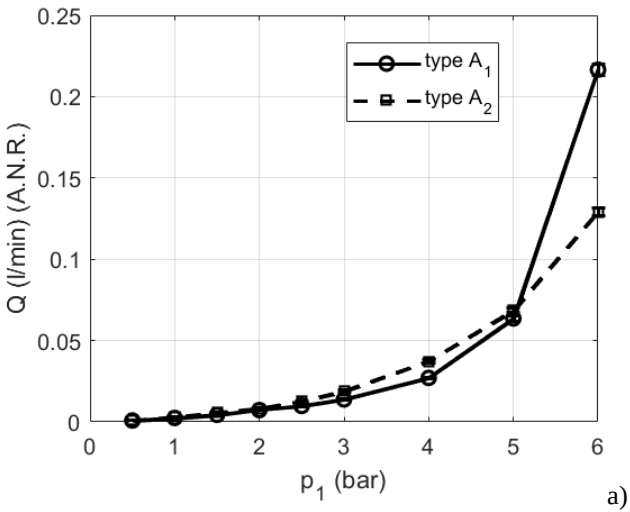

a)

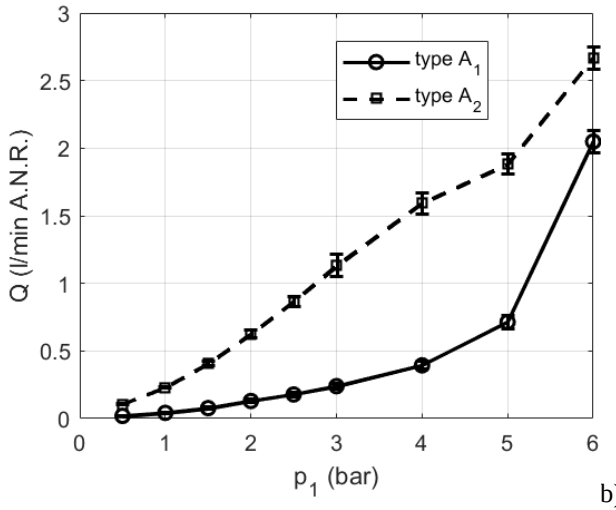

Figure 8: Leakage flow rate vs supply pressure (non-conventional tapered ring), a): 50.0 mm bore; b): 50.2 mm

For both seal types A_1 and A_2, Figures 8a and 8b show the results obtained with two different interference values, using bore diameters of 50.0 mm and 50.2 mm respectively and, consequently, different initial preloads. As can be seen from the figures, preload has a major influence on conventionally installed seal lips. Leakage flow rate across the seals increases significantly as assembly interference, and thus initial preload, is reduced.

For any given preload, leakage flow rate is lower with seal A_1 than with seal A_2, an effect which becomes more evident as bore diameter D increases. The authors believe that this can be explained by the difference in seal material stiffness, as the more flexible virgin PTFE seal (A_1) adapts better to the barrel contact surface and thus provides more effective sealing. However, if the initial preload is sufficiently high, as in Figure 8a, the flow rates for both seal types are in practice similar if compared with those in Figure 8b. Overall stiffness and lip material stiffness was measured for seals A_1 and A_2 as described in Section 4 below.

For the more flexible seal A_1, the slope of the flow rate curve rises sharply after passing approximately 5 bar. Beyond this threshold, the surface areas in contact with the barrel are significantly smaller, as pressure prevails over the preload. In particular, if D=50 mm the flow rate across seal A_1 is greater than with seal A_2.

3.2 Friction force measurement

To assess the proposed design's effectiveness, piston seal friction forces were measured at varying cylinder chamber pressures using the setup shown in Figure 9. Pressure p_1 in the chambers of cylinder (1) is regulated by pressure reducer (2) and read on gauge (3). Friction force is measured by dynamometer (4) while pulling the piston at constant speed.

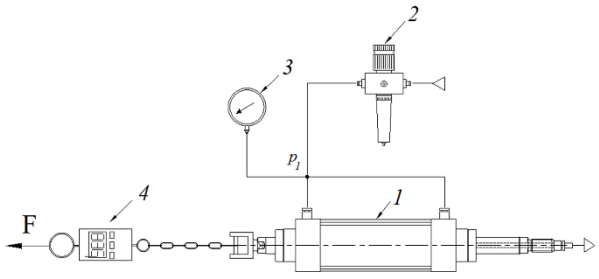

Figure. 9: Friction force test setup

Tests were carried out with the conventional and non-conventional installation configurations and two bore diameters. For the non-conventional installation, tests were also conducted without the tapered ring for purposes of comparison and in order to assess performance. Results for the 50.0 mm bore are shown in Figure 10. The friction forces shown in the graphs are for a pair of seals.

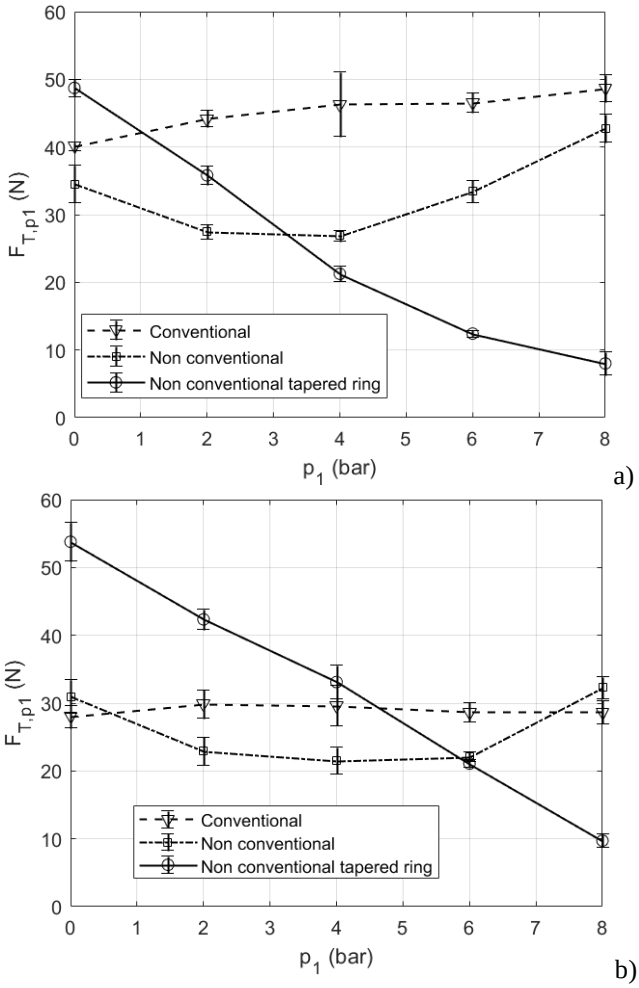

Figure 10: Friction forces, bore D = 50.0 mm, a) type seal A_1 ; b) type seal A_2

With the conventional installation, friction force increases along with chamber pressure only for seal A_1. With graphite-filled seal A_2, friction force shows little sensitivity to supply pressure, confirming this seal's greater stiffness compared to the virgin PTFE unit.

For the non-conventional installation without tapered ring, friction forces are lower than with the conventional installation. Because of irregular seal movements, however, friction forces drop to a minimum in the neighborhood of supply pressures around 3-4 bar, and then rise again as pressures increase. With the tapered retaining rings, friction forces continue to drop along with supply pressure, though this installation configuration becomes more advantageous than the other at pressures over 3-4 bar for type A_1, and 6 bar for type A_2. The non-conventional installation's advantage over the conventional configuration in terms of reducing friction force is greater for virgin PTFE seal A_1 both with and without the tapered ring. Friction forces with the 50.2 mm bore for all installation configurations are shown in Figure 11. With the larger bore, and hence lower radial interference x_0, seal A_1 with tapered ring shows an advantage earlier, at pressures over 2 bar. For seal A_2 with tapered ring, friction force is lower than with the 50.0 bore (Figure 10), but this configuration shows better performance than the same seal without tapered ring only at pressures over 6 bar.

As can be seen from Figures 10 and 11, the initial friction forces after installation show slight variations for the configuration without tapered ring, as the seal is freer to move. These variations are greater for the smaller 50.0 mm bore. In fact, when the piston-seal assembly is inserted in the barrel, the friction forces resulting from interference are higher. As a result, the initial seal position cannot be controlled. With the larger 50.2 mm bore, the phenomenon is less pronounced.

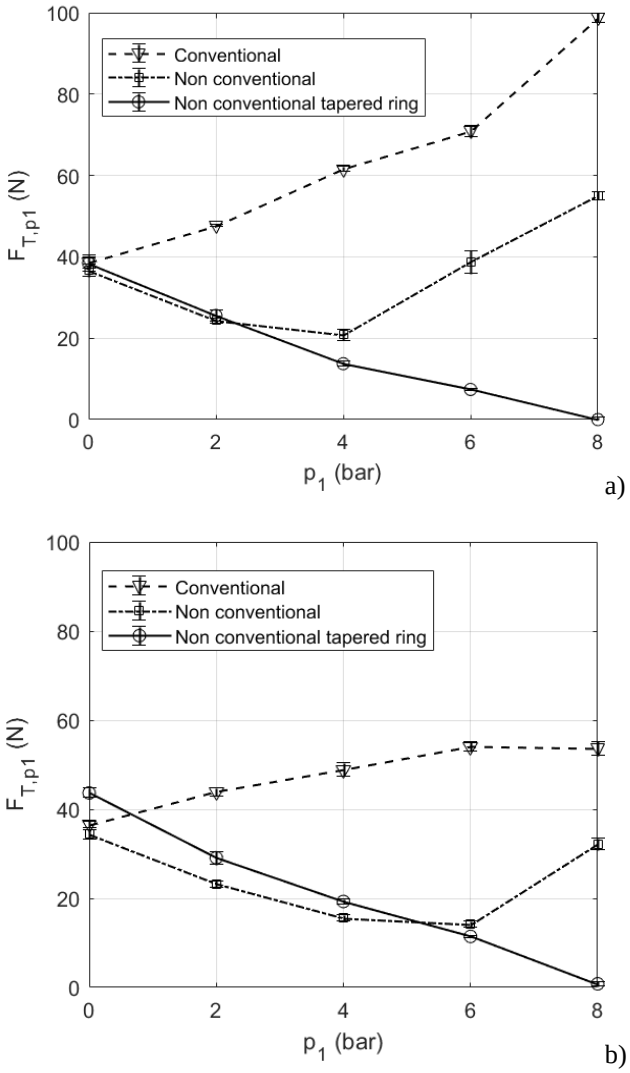

Figure 11: Friction forces, bore D = 50.2 mm; a) type seal A_1 ; b) type seal A_2

For the configuration with tapered ring, the fact that the ring prevents axial seal movement means that the lip assumes a set position upon insertion which determines the initial force.
The significantly higher friction force with the 50.2 mm bore is due to the seal's radial expansion, which positions the lip at an angle where it is more likely to bind and thus increase the friction force.
It should be emphasized that reducing the radial interference on assembly significantly lowers the friction forces on the piston, but air consumption increases.

4 Seal stiffness and friction coefficient measurement

The fact that there is friction force between the seal and barrel confirms that they are in contact at all supply pressures (Figure 10, 11). The reduction in friction force and normal contact force that takes place with rising supply pressure causes an increase in air flow to exhaust. These two effects are compatible with a reduction in the seal-barrel contact area. It is believed that leakage paths are formed between the contact surfaces' macro- and micro-asperities, resulting in partial contact at the seal-barrel interface. In [23, 24], this behavior was modeled using a soft mixed lubrication scheme and percolation theory. Lip stiffness, which results from the elasticity of the cantilever spring and the seal material, thus has a decisive role in ensuring partial contact at the interface while reducing friction and keeping leakage flow within acceptable limits. The lip stiffness needed for this purpose was estimated experimentally on seals A_1 and A_2.
A specially designed seal carrier was constructed in order to reproduce actual operating conditions. The carrier is a compact fixture holding a test specimen (PTFE and metal spring) produced by cutting a circular segment of length *Ls* from an annular seal. Figure 12a shows a photograph of the test setup, which uses an Anton Paar Model TRB tribometer. Seal specimen (1) is installed in radial contact with a 50 mm diameter barrel specimen (2) cut from the same pneumatic cylinder used for the leakage and friction force tests (Section 3.1 and 3.2). Seal carrier (3) is secured to tribometer arm (4), while normal (radial) force F_N is obtained by means of calibrated weights (5). Arm (4) is equipped with a transducer

to measure arm displacement, i.e., lip deflection x under normal force. This force was selected in order to reproduce the actual seal precompression resulting from interference fit in the barrel (x_0 in Table 1). The detail at upper left in Figure 12a shows the seal specimen of length *Ls* installed in its seat, while the detail at upper right shows a cross section of the seal, direction of deflection x and normal force F_N.

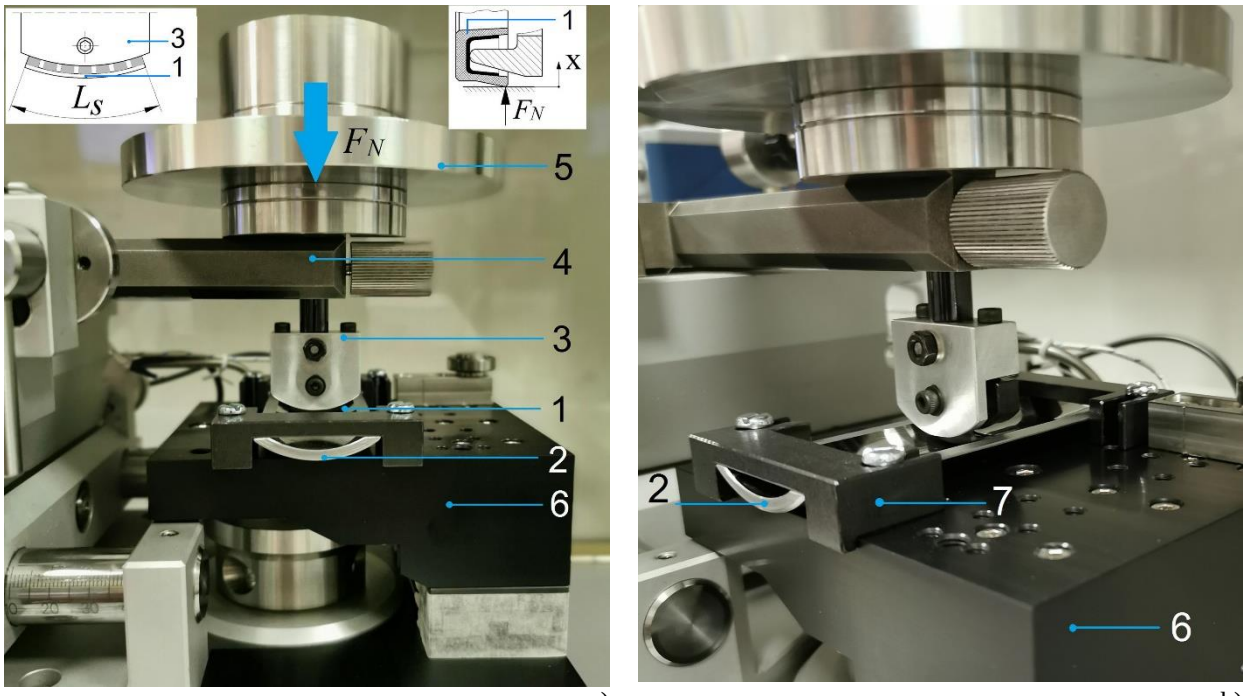

a) b)

Figure 12: Seal stiffness and friction coefficient measurement setup

Normal force F_N on seal specimen was gradually increased to reach a deflection equal to the interference fit, and then gradually reduced to zero. Measurements were repeated on at least three specimens for each seal A_1 and A_2. For both types, the increase in *x* is practically linear, indicating that seal stiffness *K* is almost constant. Figure 13 shows an example of the *x* vs. F_N curve for seal A_1.

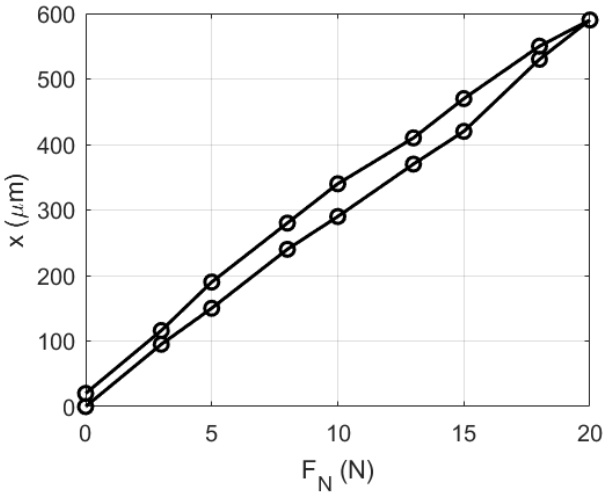

Figure 13: Deflection x versus force F_N for seal A_1, segment of length L_S

As spring and lip material elasticity can be considered to contribute in series, the *K* value thus measured is the total stiffness. Stiffness *K* and the friction coefficient were used to develop the preliminary lumped parameter model described in Section 5.

Accordingly, the tribometer was also used to measure friction coefficient f between seal and barrel while varying applied normal force. As can be seen in Figure 12b, seal carrier (3) is stationary and positively connected to tribometer arm (4), while barrel specimen (2) is secured to the tribometer's linear module slide (6) by means of fasteners and locators (7). Slide (6) is capable of linear reciprocating movement along the axis of barrel (2). Measurements were carried out at a mean velocity of approximately 0.01 m/s, similar to that used for the friction force measurements described in Section

3.2. During measurement, the tribometer gives the instantaneous friction coefficient f as the ratio of the tangential force transferred from the seal to tribometer arm (4) to the applied normal force.
Results of the tribometer measurements carried out on at least three specimens of seals A_1 and A_2 using a 50.0 mm diameter barrel specimen are summarized in Table 2. Mean radial stiffnesses per unit of circumferential length (1 mm), $K_u = K/(\pi D)$ for both seals are close to 2 N/mm^2, chiefly because they both feature the same type of cantilever spring. Measurements show a standard deviation of around 15% of the mean, in connection with seal manufacturing tolerances and the uncertainty in measuring the cantilever spring and seal specimen (the cut edge was not always perfectly radial/straight and free from burrs). The table also shows mean friction coefficients measured with radial loads of 3 to 20 N; here, the standard deviation for the three specimens is within 20 % of the mean.

Table 2 Mean tribometer stiffness and friction coefficient readings

	A_1	A_2
K_u (N/mm^2)	2.10	1.88
f	0.15	0.18

To check their reliability, friction forces measured on the tribometer were compared with those measured on the cylinder at zero supply pressure (Section 3.2). There were no significant discrepancies between measurements on a circular specimen and measurements on the complete seal.
Table 3 shows the mean friction forces in both cases; given that these forces are those for a single seal, the values shown for the seal as installed in the pneumatic cylinder were obtained by dividing the forces shown at supply pressure $p_1 = 0$ in Figure 10 by two. F_{T,L_s} is measured with the circular segment of length L_s mounted on the tribometer, while F_T is the corresponding friction force extended to the entire length of the seal: $F_T = (F_{T,L_s})\frac{2\pi R}{L_s}$, where R is the barrel radius. The good correspondence between F_T measured on the tribometer and $F_{T,p_1=0}$ measured with the pneumatic cylinder confirms the value of the tribometer measurement setup and the seal specimen's ability to reproduce actual operating conditions.

Table 3: Comparison of friction forces measured on the tribometer and on the pneumatic cylinder (single seal), bore diameter 50.0 mm

	$F_{T,p_1=0}$(N)	x_0 (micron)	L_s (mm)	F_{T,L_s} (N)	$F_T = (F_{T,L_s})\frac{2\pi R}{L_s}$ (N)
A_1	24.35	570	16.25	2.85	27.55
A_2	26.90	610	16.02	3.24	31.40

5 Preliminary lumped parameter model of the seal lip

A preliminary lumped parameter model was developed to gain a better understanding of the seal lip's behavior under load. The model reproduces this behavior at the macroscopic level.
For simplification, the lip is schematized as a rigid body which under external load rotates around the end connected to the outside face. Cross sections of the seal both free and installed in the barrel are shown in Figure 14a, where L is the lip, F is the outside face, S is the cantilever spring, x_0 is radial interference, and y is the coordinate measuring lip movement from the original installation position. Positive values of y mean that the lip has separated from the barrel. The model is shown schematically in Figure 14b. Three lumped forces act on the lip: air pressure thrust force F_P which acts to separate the seal from the barrel, seal spring elastic reaction force F_e, and seal-barrel contact force F_c. As explained in Section 3.1, seals are installed in such a way that pressure can deflect the lip without causing axial movements, thanks to tapered ring *A*): lip movement can thus be represented as a rotation about the virtual hinge O.

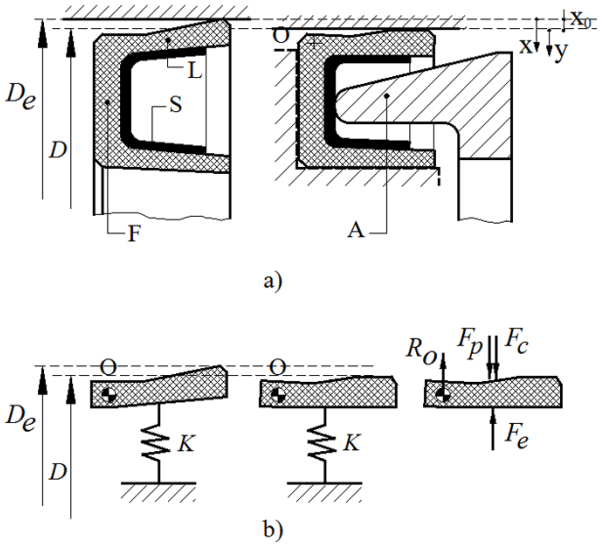

Figure 14: a) Schematic views of free and installed seal. b) Simplified lumped parameter model

The rotational equilibrium equation yields:

$$F_P + F_c - F_e = 0 \tag{1}$$

where elastic force F_e is given by:

$$F_e = K\,x = K(x_0 + y) \tag{2}$$

These expressions give:

$$F_P + F_c = K(x_0 + y) \tag{3}$$

In the initial installation condition (y=0) with zero supply pressure (p_1=0), equation (3) gives the maximum contact force generated by seal interference fit x_0:

$$F_{c,0} = K\,x_0 \tag{4}$$

Equation (3) can be rewritten to account for the discontinuity resulting from the fact that contact force F_c drops to zero for $y > 0$; bearing equation (4) in mind, we have:

$$\begin{cases} F_P = F_{c,0} + Ky & y > 0 \quad (a) \\ F_P = F_{c,0} - F_c & y \le 0 \quad (b) \end{cases} \tag{5}$$

It is clear from equation (5) that the pressure force F_P required to separate the seal lip from the barrel is $F_P = F_{c,0}$, or in other words, equal to the maximum preload force generated by the spring. With this pressure force, we obviously have $F_c = 0$, as can again be seen from equation (5). Bearing in mind the friction relation between contact force and tangential force, we have:

$$F_{c,0} = \frac{F_{T,p_1=0}}{f};\; F_c = \frac{F_{T,p_1}}{f}$$

where $F_{T,p}$ and $F_{T,p_1=0}$ are the friction forces in the barrel at the generic supply pressure and at zero supply pressure ($p_1 = 0$) respectively.
Substituting the two relations above in equation (5) gives:

$$\begin{cases} F_P = F_{T,p_1=0} + Ky & y > 0 \quad (a) \\ F_P = \frac{F_{T,p_1=0}}{f} - \frac{F_{T,p_1}}{f} & y \le 0 \quad (b) \end{cases} \tag{6}$$

Experimental data for friction force with and without supply pressure, $F_{T,p_1=0}$ and F_{T,p_1}, were inserted in formula (6). In particular, data was used from the measurements on seal A_1 and D=50.0 mm shown in Figure 10. To allow for the friction contribution of a single seal, the measurements from Figure 10 were divided by two. Results are shown versus coordinate x in Figure 15a. As can be seen, contact force F_c drops from initial value $F_{c,0}$ with no supply pressure, reaching zero when pressure force F_p overcomes force $F_{c,0}$ and the lip begins to separate from the barrel. As equation (6b) applies from this point, the pressure force increases linearly with deflection x. In Figure 15b, the same results are shown versus supply pressure p_1; as can be seen, the lip has not yet separated completely from the barrel at maximum test pressure p_1. In addition to the experimental points, Figure 15a shows the points corresponding to lip separation (where $F_c = 0$, $y = x_0$, $F_p = F_e$); these points were extrapolated, as F_c and F_p increase linearly with x. It should be pointed out, however, that according to this model the increase in pressure p_1, and hence in force F_p, does not deflect the cantilever spring in the $0 \le x \le x_0$ ($y \le 0$) range, i.e., in the deflection range at installation. Rather, there is a recovery in force, such that when $F_p = F_{c,0} = K\,x_0$, contact force drops to zero ($F_c = 0$); this is the condition corresponding to the onset of complete separation between seal and lip. Consequently, the deflection values shown in Figure 15a for the $0 \le x \le x_0$ range are fictitious.

The friction forces measured on the pneumatic cylinder and the friction coefficients measured with the tribometer shown in Table 2 can then be used to calculate seal stiffness and compare it with the tribometer stiffness reading. Specifically, as the experimental values for contact force $F_{c,0}$ and interference fit x_0 are known for each seal type, equation (4) gives a stiffness K_u of 1.78 N/mm^2 and 1.60 N/mm^2 for seals A_1 and A_2 respectively. Allowing for friction coefficient and friction force measurement uncertainty, results are in line with those obtained on the tribometer (see Table 2).

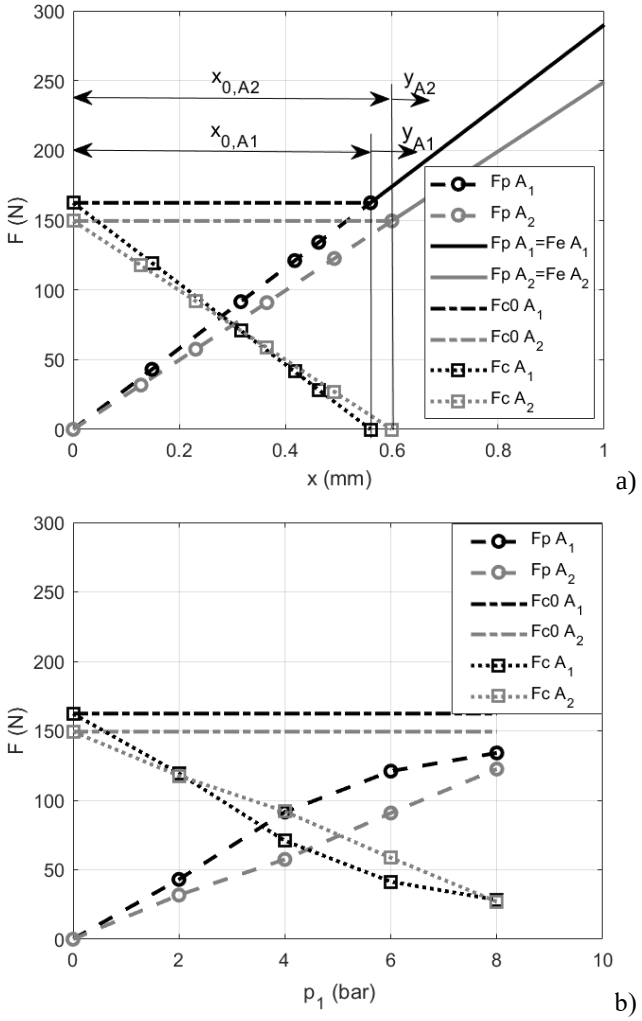

Figure 15: Contact and pressure forces on seal lip: a) versus coordinate *x*; b) versus supply pressure p_1

6 Leakage flow rate and equivalent air gap

Together with the experimental values for stiffness K and friction force, the lumped parameter model presented above provides a macroscopic view of seal behavior. The results are consistent at the level of exchanged forces and make it possible to distinguish the lip/barrel contact area ($x \leq x_0$ in Figure 15a) from the area where the interface surfaces are completely separated. However, the model's simplification precludes a microscopic analysis of contact which, as is usually the case with contact surfaces, takes place between the asperities resulting from the bodies' surface roughness ("partial contact"). A possible schematization of the two surfaces' contact interface is shown in Figure 16. The dark spots represent the contact regions, while the white areas are the valleys that serve as supply pressure paths.

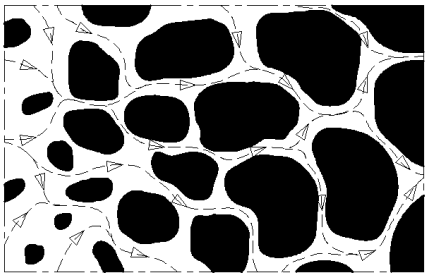

Figure 16: Schematization of the contact interface

Behavior as represented in Figure 16 is confirmed by the measurements in Figure 10, given that leakage flow also occurs in the range of pressures p_1 in which the model discussed in Section 5 contemplates contact between lip and barrel ($F_p \leq F_{c,0}$). Because of the foregoing considerations and the nature of the materials and surfaces involved, radial interference is unable to prevent air from leaking across the seal. This, however, undoubtedly helps the non-conventional installation configuration presented herein to achieve its low-friction performance aims.

The micro-scale mathematical models developed in [23, 24] provide a highly accurate evaluation of flow behavior in the contact region. As air flow through the narrow winding channels can be likened to flow across porous media, the modified Darcy equation [25] could be used to identify the behavior of the porous resistances. In the case in question, however, porosity is difficult to evaluate because the contact regions are not evenly distributed along the direction of flow.

The simplified lumped parameter approach presented in Section 5 can be used to identify two springs, viz., for seal material stiffness K_M and cantilever spring stiffness K_S. The schematization used for the seal installed in its seat under initial preload conditions is shown in Figure 17a; here, lip deformed geometry is obviously qualitative. The profile as measured with an SM Instruments Model PGS 200 stylus profilometer is represented in Figure 17b, which shows the main axial dimensions together with nominal bore diameter D=50.0 mm. Given the shape of the profile and the clearances between the seal and the barrel, contact will take place over a length which is less than the seal's total length. This contact length, designated as L_c in Figure 17, was estimated as the distance from the intersection of the outside lip surface and the horizontal line representing the bore to the intersection of the inside and outside lip surfaces.

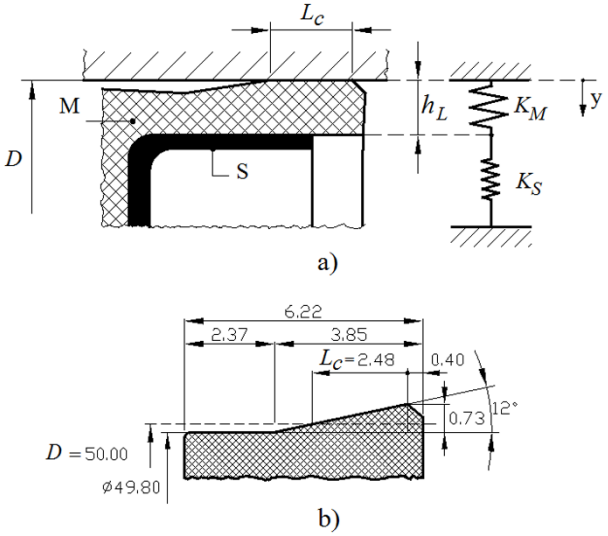

Figure 17: a) Lumped parameter model of the seal (springs in series), b) Cross-section of the free seal as measured on profilometer

The leak rate calculation method proposed here envisages that in the fluid pressure range in which partial contact takes place between seal and barrel, increasing supply pressure will open new channels between the ridges and valleys in the

seal material, thus gradually reducing the areas where the latter contacts the barrel. In this stage, seal material stiffness K_M has a key role in determining the area of the channels through which leakage flow escapes to exhaust. Figure 18a is a schematization of the partial contact region and the leakage channels between the ridges and valleys; the springs indicate material stiffness in the lumped parameter approach. How stiffness affects the material's behavior can be identified case by case. For example, a soft seal material will show excellent compliance with the asperities on the barrel's hard countersurface, but will be more likely to allow leakage channels to open as pressure p_1 is increased.
Leakage at the seal-barrel interface can be modeled qualitatively and quantitatively as flow across an equivalent constant height air gap. A model of this kind idealizes partial contact at the interface separated by a thin film crossed by fluid. The lumped parameter model used for this purpose is shown in Figure 18b: deformation of the seal material and thus of spring K_M creates flow in an air gap of uniform height δ_{eq} along the contact length.

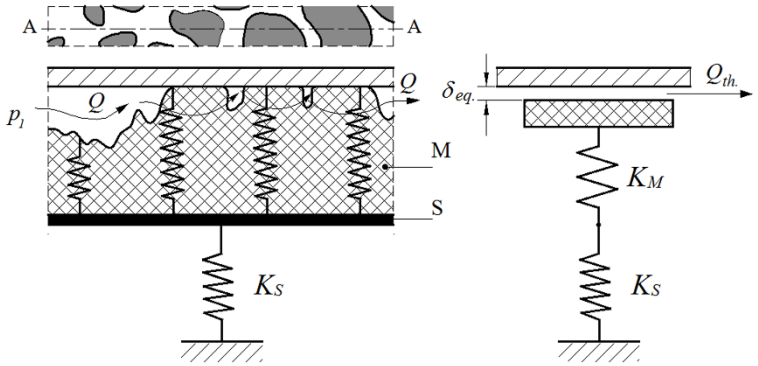

Figure 18: Lumped parameter schematization of contract region and equivalent air gap

The theoretical flow rate Q_{th} across this air gap was calculated using equation (7), obtained by integrating the Reynolds equation for one-directional laminar and isothermal flow [11].

$$Q_{th} = \frac{2\pi D}{24\mu R T L_c}\,\delta_{eq}{}^3\left(P_1{}^2 - P_a{}^2\right)\frac{1}{\rho_N} \qquad (7)$$

Q_{th} is the volumetric flow rate at standard reference atmosphere (ANR) with a double-seal installation, μ is the dynamic viscosity of air, R is the air constant, T is temperature (293 K), P_1 and P_a are the absolute supply and exhaust pressures respectively, and ρ_N is ANR air density.
Stiffness K_M was determined on the basis of the elastic and geometric properties of the elastically deformed contact are; specifically:

$$K_M = \frac{E\,A_c}{h_L} \qquad (8)$$

where E is the material's elastic modulus, A_C and h_L are the lip contact area and thickness respectively; the following expression applies to the contact area: $A_c = \pi D L_C$
The elastic modulus was measured experimentally by means of instrumented Vickers microindentation tests (Anton Paar model NHT^3 nanoindentation tester): tests were carried out on the seal specimens used for stiffness and friction measurements, with the indenter applied to the flat surface of the outside face.
The elastic modulus readings and the stiffness values obtained with equation (8) for both seal types are shown in Table 4. Stiffness is expressed per unit of circumferential length: $K_{M,u} = K_M/(\pi D)$. As can be seen by comparing Table 4 and Table 2, seal material stiffness is much higher than cantilever spring elastic stiffness. Consequently, total stiffness K (Section 5) will be very close to cantilever spring stiffness (given that the springs are in series). It is thus reasonable to assume that the deformation resulting from interference fit x_0 is almost entirely absorbed by the cantilever spring, i.e., the element with lower stiffness. Increasing pressure $p_1$will act on the preloaded lip by lifting it away from contact until the two surfaces separate ($F_c = 0$); plausibly, the pressure force acting on the seal material micro-asperities compresses the ridges to open new air channels, with a corresponding increase in leakage flow rate.

Table 4 Mean elastic modulus and stiffness of seal material

	A_1	A_2
E (N/mm²)	485	880
$K_{M,u}$ *(N/ mm²)*	1002	1820

The height of the equivalent air gap was thus determined by calculating material deformation under pressure force F_P:

$$\delta_{eq} = \frac{F_p}{K_M} \tag{9}$$

The values of force F_P to be introduced in equation (9) were calculated using formula 6b). These values also appear in the "partial contact" region of the graph in Figure 15, i.e., in the range where $0 \leq x \leq x_0$ ($y \leq 0$). Entering the values given by formula (9) in formula (7) yields the theoretical leakage flow rate. Figure 19 shows results for both seals A_1 and A_2 with nominal bore diameter D=50.0 mm; as can be seen, there is a good fit between experimental measurements and the theoretical results of the equivalent air gap model.

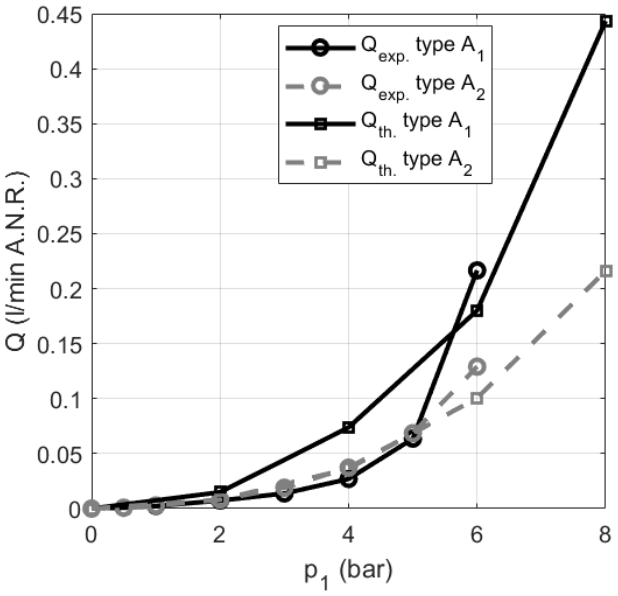

Figure 19: Theoretical and experimental leakage flow rate

7 Conclusions

Leakage flow rate and friction force was measured versus bore diameter and supply pressure on two types of non-conventionally mounted lip seals. A tribometer equipped with a purpose-built seal carrier pin was used to measure seal material friction coefficient and the lip's elastic stiffness. These magnitudes were the basis for developing a simplified lumped parameter model whereby the exchanged contact forces and leakage flow rate between seal and barrel were determined. Despite the simplifying assumptions, the good fit between theoretical and experimental leakage flow rate confirmed the model's worth.

Tests indicated that the non-conventional installation configuration is effective as a simple, economical means of reducing friction forces in pneumatic cylinders. Appropriate axial retention for the seal provided better performance than simply reversing the seal assembly position. Test results confirmed that the non-conventional installation is a promising route for reducing friction force. Further research must necessarily center on a careful choice of seal shape and material in order to ensure a level of radial stiffness that balances the need to reduce friction forces with an economically acceptable leakage flow rate. The model presented herein can be an effective tool for that purpose, and can be used both to redesign the tested seals and to design and evaluate similar lip seals once geometric parameters, stiffness and friction coefficient are known. While the model in its current state is a good starting point, better results can undoubtedly be achieved in the future by increasing its complexity.

References

[1] Calvert, C., Tirovic, M, Stolarski, T. Design and development of an elastomer-based pneumatic seal using finite-element analysis, J.Eng.Tribol. 216(J3), 127–138.T (2002).

[2] Belforte, G., Manuello, A., Mazza, L. Optimization of the cross section of an elastomeric seal for pneumatic cylinders, J.Tribol.128, 406–413 (2006).

[3] Wangenheim, M., Kozma, M., Mate, L., Gronefeld, P., Friction behaviour of grease lubricated seals, Proceedings of the 15th International Sealing Conference, Stuttgart, Germany, 7-8 October, 265-280 (2008).

[4] Belforte, G., Conte, M., Manuello, A., Mazza, M. "Performance and behavior of seals for pneumatic spool valves", Tribology Transactions, 54, 237-246 (2011).

[5] Hermann, A., Dabisch, T., Influence on tribological behaviour of pneumatic actuators due to modifications of polymer compounds, Proceedings of the 15th International Sealing Conference, Stuttgart, Germany, 7-8 October, 265-280 (2008).

[6] Pei, Y.T., Bui, X.L., Zhou, X.B., De Hosson J.Th.M., Tribological behavior of W-DLC coated rubber seals, Surface and Coating Technology, 202, 1869-1875 (2008).
[7] Verheyde, B., Havermans, D., Vanhulsel A., Characterization and Tribological Behaviour of Siloxane-based Plasma Coatings on HNBR Rubber, Plasma Processes and Polymers, 8, 755-762 (2011).
[8] Conte, M., Igartua, A. Study of PTFE composites tribological behavior, Wear 296, 568-574 (2012).
[9] Etsion, I., Hamrock, B.J. Optimum step design for centering of pistons moving in an incompressible fluid. J. Fluids Eng., 99 (4), 675-680 (1977).
[10] Belforte, G., Ferraresi, C., Raparelli, T., Trivella, A. New design of low friction cylinders. 12 Aachener fluidtechnisches colloquium. Aachen (Germany), 12-13 March 1996. pp. 629-642.
[11] Belforte, G., Raparelli, T., Mazza, L., Trivella, A. Analysis, design and comparison of different types of pistons for sealless pneumatic cylinders and valves. Tribol. Trans., 48, 377-388 (2005).
[12] Etsion, I. Analysis and design of a uniform-clearance pumping ring rod seal for the Stirling engine. J. Mech. Design, 107, 67-72.
[13] Ronen, A., Etsion, I., Kligerman, Y. Friction-Reducing Surface-Texturing in Reciprocating Automotive Components. Tribol. Trans., 44 , 359-366 (2001),
[14] Ryk, G., Etsion, I. Testing piston rings with partial laser surface texturing for friction reduction. Wear 261 (2006), pp. 792–796.
[15] Belforte G., Mazza, L., Visconte, C. Design methodology for an air lubricated seal, Trib. Int., 75 (2014), pp. 104-110.
[16] Belforte, G., Ferraresi, C., Raparelli, T. A new low-friction pneumatic actuator, 2nd Int. Symp. On Fluid Power, Transmission and Control, Shanghai, 1995.
[17] Raparelli, T., Mazza, L., Trivella, A. Study of a non-conventional sealing system for low-friction pneumatic cylinders. Proceedings - Tribology and Design 2012, Kos, Greece, 2012, pp. 55-64.
[18] Bulut, T., Temiz, V., Parlar, Z. The effect of interference on the friction torque characteristics of TPU based rotary lip seals, Tribology in Industry, 37 (2015), pp. 346-353.
[19] Belforte, G., Conte, M., Mazza, L. Low fiction multi-lobed seal for pneumatic actuators, Wear, 320, pp 7-15, (2014).
[20] Belforte, G., Conte, M., Manuello, A., Mazza, L. “Performance and behavior of seals for pneumatic spool valves”, Tribology Transactions, 54, pp. 237-246, (2011).
[21] Raparelli, T., Mazza, L., Trivella, A. Non-conventional lip seal mountings for pneumatic cylinders, ECOTRIB 2015, Lugano, Switzerland, 2015.
[22] Raparelli, T., Mazza, L., Trivella, A. Experimental tests on non-conventional lip seal for pneumatic cylinders, ECOTRIB 2017, Ljubljana, Slovenia, 2017.
[23] Scaraggi, M., Carbone, G. A Two-Scale Approach for Lubricated Soft-Contact Modeling: An Application to Lip-Seal Geometry. Advances in Tribology, Vol. 2012, Article ID 412190, doi:10.1155/2012/412190.
[24] Lorenz, B., Persson, B. N. J. Leak rate of seals: Comparison of theory with experiment. EPL, 86 (2009) 44006 doi: 10.1209/0295-5075/86/44006.
[25] Hunt, A., Ewing, R., Ghanbarian, B. Percolation Theory for flow in porous media. Lecture Notes in Physics, (2014) Springer doi: 10.11007/978-3-319-03771-4.